DOI: 10.13009/EUCASS2022-6180

Impact of a Formation Flight Wake-Tracking Strategy on the Dynamics of the Downstream Wake

Ignace Ransquin⋆*, Matthieu Duponcheel⋆†, Denis-Gabriel Caprace⋆‡ and Philippe Chatelain⋆§
⋆ *Institute of Mechanics, Materials and Civil Engineering*
Université catholique de Louvain, 1348, Louvain-la-Neuve, Belgium

Abstract

Formation flight is known to improve the efficiency of a two-aircraft formation provided that the follower is able to surf the wake of the leader. An accurate tracking of the leader's wake position is thus mandatory in order to perform efficient extended formation flight that better addresses safety concerns for civilian applications. This energy-efficient flight strategy leads however to different wake dynamics compared to those of the wake of an isolated aircraft. Even more, the uncertainty on the relative position between the follower and the wake of the leader that is inherent to any tracking strategy, further increases the complexity of the underlying vortex dynamics. This paper presents a methodology that seeks to describe the propagation of the wake of a formation, from the tracking of the leader's wake by the follower, to the long-term wake evolution through the use of Large Eddy Simulations (LES). The wake sensing strategy exploited by the follower makes use of measurements of its entire six degrees-of-freedom dynamics in order to track the position of the leader's wake. A calibrated combination of space developing and time developing simulations then enables to capture the roll-up of the vortex sheets originating from the leader and the follower, their mutual interactions and their long term evolution in a turbulent environment. The entire methodology is applied to a representative configuration involving two long-haul aircraft in formation flight.

1. Introduction

Birds have been occupants of the sky long before mankind began to gradually appropriate it too. Thanks to the work of evolution, different species have been able to progressively develop and learn the most inventive techniques to optimize different flight objectives. For instance, birds of prey use soaring to maintain an elevated vantage point in their search for food. The formation flight technique performed by migratory birds in order to reduce their energy consumption is another example. In the latter, following birds in the formation indeed benefits from substantial apparent drag reduction when flying in the upwash region of the leaders' wake.[26,35] To maintain such impressive V-shaped formations, birds have the ability to *sense* the upwash region induced by the wake produced by the leading birds. Consequently, they minimize their energy expenditure by flying in the aerodynamically optimal position, as shown by Portugal et al.[31]

Just like birds flying in flocks, the synchronized flight of aircraft is a way of organizing the sky and a promising method for many new opportunities. The development of close formation flight has allowed, for example, to increase the range of operability of military aircraft through aerial refueling.[20] For civilian applications, the new concept of extended formation flight[30] is more appropriate than close formation flight as it better adresses safety concerns. This bio-inspired technique can lead to significant fuel savings as recently showed in commercial aviation.[1,22] In that case, the follower is flying several tens of wingspans downstream of the leader and still benefits from a positive interaction. However, an accurate tracking of the wake position is thus mandatory in order to perform efficient formation flight, as it has been shown that 50% of the benefit is lost if the follower cannot maintain a lateral and vertical relative position within 10% span of the leader.

Several methods allowing the follower to track the vortices have been proposed in the literature from the direct measurement of the flowfield[15,28] to peak-seeking or Kalman filter-based wake tracking strategies.[11,19,23] This paper builds upon,[32] where the authors propose a wake tracking strategy based on measurements of the aircraft dynamics.

*Ph.D. Candidate; ignace.ransquin@uclouvain.be.
†Research Engineer, Ph.D.
‡External scientific collaborator, Ph.D.
§Professor.

DOI: 10.13009/EUCASS2022-6180

Whereas the characteristics of the tracking strategy were studied in details in their work, we here investigate the impact of a wake tracking strategy on the fare wake evolution over time through the use of Large Eddy Simulations (LES).

Indeed, another key research area relates to the study of the evolution of the wake produced by an aircraft formation as that dynamic will govern the air traffic management decisions. While the propagation the two-vortex system that emanates from an isolated aircraft has long been studied,[18,24] the wake of a formation shows different behavior with an important sensitivity to the relative position of the aircraft. This has already been highlighted in[34] where the authors performed Time Developing LES of two pairs of rolled-up vortices in order to study the far-field wake evolution.

In this paper, we use the state-of-the-art LES flow solver, called Vortex-Particle-Mesh method (VPM)[8] and a calibrated combination of 3D Space Developing (SD) and 3D Time Developing (TD) simulations to capture the roll-up of the vortex sheets originating from the leader and the follower, their mutual interactions and their long term evolution in a turbulent environment.[33] The 6 degrees-of-freedom dynamics of the leader and the follower are accounted through in the VPM simulations. By measuring its dynamics, the follower estimates the position of the wake of the leader, and tracks it in order to maintain a constant relative position.[32] We study the consequences and constraints induced by the formation wake for the air traffic management, e.g., in terms of vortex propagations and dissipation.

In this work, we rely on both a high-fidelity simulated flight environment of two aircraft in formation based on LES in order to produce simulated flight datas and a surrogate model that reproduces the aerodynamics of the formation in a simplified manner. This surrogate model is exploited by an estimator in order to compare measurements provided by the simulated flight environment and to predict the position of the leader's wake over time. The structure of this paper is as follows. The wake tracking strategy based on dynamic measurements of follower aircraft is presented in Section 2. We then present in Section 3 the methodology that combines Space Developing and Time Developing (TD) simulations in order to be able to observe the wake evolution over long distances. In Section 4, we present simulation results. We conclude this paper with some conclusions in Section 5.

2. Kalman filter-based wake tracking strategy

The focal idea of this paper is to combine both a wake tracking strategy that enables efficient formation flight and the simulation of the long-term evolution of the resulting formation wake over time. This starts with the estimation of the wake position following a similar framework as the one presented by Ransquin et al.[32] An estimator makes use of an Ensemble Kalman Filter (EnKF) in order to process dynamic measurements computed by the simulated flight environment and to estimate the position of the wake that impacts the follower. This is done through the exploitation of a state-space representation of the formation, namely the surrogate model. The estimated wake position is used by the autopilot of the follower to maintain a constant relative position over time. Fig. 1 is a schematic representation of the complete architecture. In this section, we present the estimation strategy. First, we describe in Section 2.1 the estimator structure. Then, we present in Section 2.2 the aircraft aerodynamic model that is exploited by estimator over time.

2.1 Estimator and Kalman Filtering

This work relies on the discrete-time Kalman Filter framework to estimate the position of the wake of a leader. With regard to the estimator, this position is represented by a wake state vector $\boldsymbol{q}_{wake}$. Associated to the follower's dynamics state vector $\boldsymbol{q}_{dyn}$, they form the state vector $\boldsymbol{q}$ that is propagated by the estimator over time using the surrogate model. The propagation step produces the predicted measurement vector $\boldsymbol{m}$, which is compared with the true measurement vector $\boldsymbol{z}$ in order to produce an updated estimated state during the analysis step.

The EnKF uses a Monte Carlo approach to propagate the statistics of the states through the system. This enables to preserve the non-linearity of the system for improved performances in this formation flight complex flow environment.[23] The state vector $\boldsymbol{q}$ is thus represented by a discrete ensemble of size N. The propagation step consists in the time evolution of each member $\boldsymbol{q}_i^n$ of the ensemble from iteration n to $n+1$ through the surrogate model, i.e.,

$$\begin{cases} \mathbf{q}_i^{n+1|n} = \mathbf{f}(\mathbf{q}_i^n) \\ \mathbf{m}_i^{n+1|n} = \mathbf{h}(\mathbf{q}_i^n), \end{cases} \tag{1}$$

where $(.)^{n+1|n}$ denotes the propagation of the model without any measurements incorporated in the estimation process, and $\mathbf{f}$ and $\mathbf{h}$ are non-linear functions describing the surrogate model. *A priori* state mean and covariance are deduced

DOI: 10.13009/EUCASS2022-6180

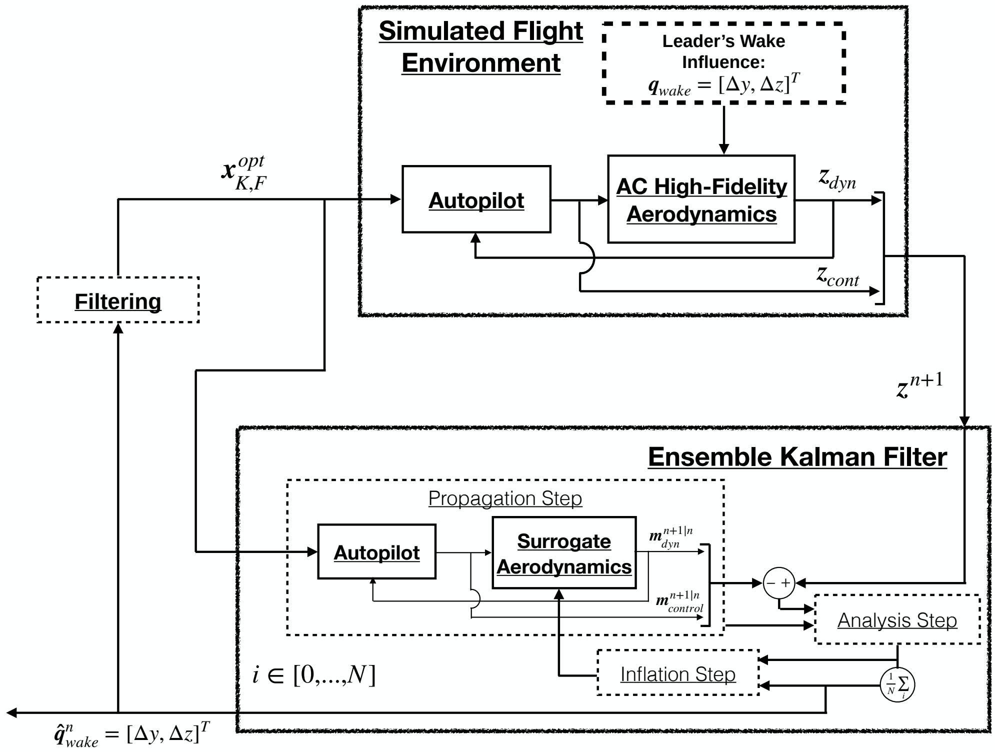

Figure 1: Block diagram of the tracking strategy including the simulated flight environment, the estimators and a filtering tool to provide a smooth target.[32]

from the ensemble, i.e.,

$$\hat{\mathbf{q}}^{n+1|n} = \frac{1}{N}\sum_{i=1}^{N}\mathbf{q}_i^{n+1|n}, \tag{2}$$

$$\boldsymbol{P}^{n+1|n} = \frac{1}{N-1}\sum_{i=1}^{N}(\mathbf{q}_i^{n+1|n} - \hat{\mathbf{q}}^{n+1|n})(\mathbf{q}_i^{n+1|n} - \hat{\mathbf{q}}^{n+1|n})^T. \tag{3}$$

The innovation step is performed by comparing the true measurements z^{n+1}, i.e., those obtained from the high-fidelity flight environment at the current assimilation time, and the measurement vector $\mathbf{m}_i^{n+1|n}$ of each element of the ensemble, i.e.,

$$\mathbf{y}_i^{n+1} = (z^{n+1} + \boldsymbol{\epsilon}_i) - \mathbf{m}_i^{n+1|n}, \tag{4}$$

where $\boldsymbol{\epsilon}_i \sim \mathcal{N}(0, \boldsymbol{R})$ is the zero-mean Gaussian measurement noise with covariance $\boldsymbol{R}$. Then, the analysis step starts with the computation of the Kalman gains $\boldsymbol{K}^{n+1}$, i.e.,

$$\boldsymbol{K}^{n+1} = \boldsymbol{P}^{n+1|n}(\boldsymbol{H}^{n+1|n})^T\left(\boldsymbol{R}^{n+1} + \boldsymbol{H}^{n+1|n}\boldsymbol{P}^{n+1|n}(\boldsymbol{H}^{n+1|n})^T\right)^{-1}, \tag{5}$$

where $\boldsymbol{H}^{n+1|n}$ is the measurement matrix obtained in the frame of an implicit linearized formulation of the observation operator $\boldsymbol{h}$.[14] In practice, it means that the measurement matrix $\boldsymbol{H}^{n+1|n}$ is not directly computed. Instead, an approximation of the products $\boldsymbol{P}^{n+1|n}(\boldsymbol{H}^{n+1|n})^T$ and $\boldsymbol{H}^{n+1|n}\boldsymbol{P}^{n+1|n}(\boldsymbol{H}^{n+1|n})^T$ can be computed given the prior ensemble.[21] Each member of the ensemble is individually updated using the Kalman gain in its classical form, i.e.,

$$\mathbf{q}_i^{n+1} = \mathbf{q}_i^{n+1|n} + \boldsymbol{K}^{n+1}\mathbf{y}_i^{n+1}. \tag{6}$$

The *a posteriori* state estimate and associated covariance matrices are deduced by taking the mean $\hat{\boldsymbol{q}}^{n+1}$ and

DOI: 10.13009/EUCASS2022-6180

covariance $\boldsymbol{P}^{n+1}$ of those ensemble members, i.e.,

$$\hat{\mathbf{q}}^{n+1} = \frac{1}{N}\sum_{i=1}^{N}\mathbf{q}_i^{n+1}, \tag{7}$$

$$\boldsymbol{P}^{n+1} = \frac{1}{N-1}\sum_{i=1}^{N}(\mathbf{q}_i^{n+1} - \hat{\mathbf{q}}^{n+1})(\mathbf{q}_i^{n+1} - \hat{\mathbf{q}}^{n+1})^T. \tag{8}$$

In the EnKF framework, process noise is not explicitly represented in the propagation step of the EnKF, see Eq. (1). Indeed, that noise is implicitly added to the ensemble members because of the Monte Carlo formulation of the EnKF.[16] Nevertheless, covariance state inflation is implemented and alters the wake state vector of each ensemble at each estimation step in a similar form to Gaussian random walk dynamics, see[25] for a more detailed description. In the context of this work, we use the EnKF to exploit its ability to handle nonlinear processes, which is required for an accurate estimation of the wake position as highlighted in[23] and.[7]

2.2 Simplified aerodynamic model

The Prandtl Lifting Line (PLL) theory constitutes the core of the simplified aerodynamic model. As depicted in Fig. 2, the follower aircraft is located at the position $\boldsymbol{x}_F = [x_F, y_F, z_F]_i^T$ in the inertial frame $(ox_iy_iz_i)$ and comprises three straight lifting lines representing the wing, the vertical tail plane (VTP) and the horizontal tail plane (HTP). In this model, the wake of an aircraft is made of one flat vortex sheet produced by the wing, and the two perpendicular vortex sheets produced by the tail due to the HTP with the VTP. All those vortex sheets are assumed to go straight to infinity.

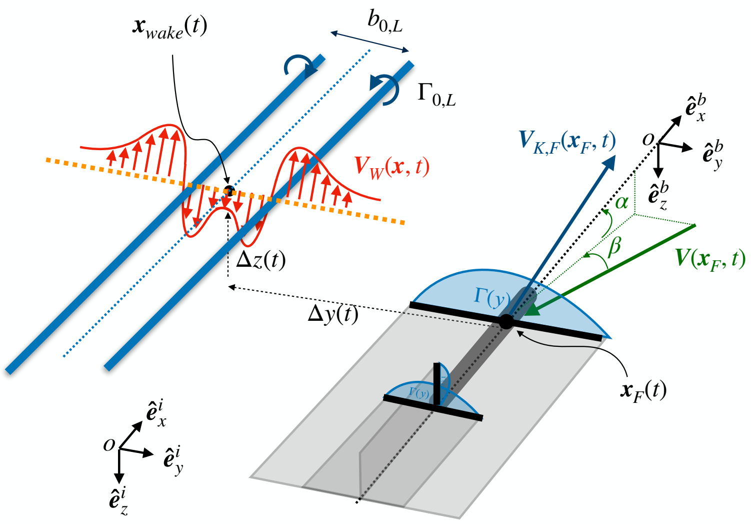

Figure 2: Aerodynamic model of the follower under the influence of a leader's wake.[32]

The wake of the leader is modeled as two counter-rotating vortex tubes of circulation $\Gamma_{0,L}$ and spacing $b_{0,L}$ located in $\boldsymbol{x}_{wake} = [x_{wake}, y_{wake}, z_{wake}]_i^T$. The upwash velocities $\boldsymbol{V}_W(\boldsymbol{x}, t)$ is induced on the follower wing and is computed using a low-order algebraic wake vortex model with a core radius $r_c/b = 0.05$.[3] Compared to what is done in,[32] we assume that $\Gamma_{0,L}$ and $b_{0,L}$ are known constant parameters that do not need to be characterized over time, i.e., the geometrical characteristics of the leader are assumed to be known. For the aerodynamic part of the model, the variables characterizing the wake of the leader are therefore its position in the (oy_iz_i) plane, i.e.,

$$\boldsymbol{q}_{wake} = [y_{wake}, z_{wake}] \; . \tag{9}$$

In this work, we focus on the lateral and vertical relative positions in the (oy_iz_i) only, neglecting the streamwise position x_{wake}. Indeed, maintaining an optimal position in the (oy_iz_i) plane is critical in order to maximize the energy savings.

Using the Prandtl lifting line theory, one computes the circulation distribution along each one of the lifting lines, solving the integro-differential equation that relates the circulation with the relative air velocities along the lines $\boldsymbol{V}(\boldsymbol{x}_F, t)$, i.e. the combination of the velocities induced by the follower flight path velocity $\boldsymbol{V}_{K,F} = [U_{K,F}, F, V_{K,F}, W_{K,F}]_i^T$, the leader's wake induced velocity $\boldsymbol{V}_W$ and the lifting lines induced velocity. Note that this constitutes a quasi-steady

DOI: 10.13009/EUCASS2022-6180

assumption, where the wake instantaneously propagates to infinity. The forces $\boldsymbol{F}_F = [F_x, F_y, F_z]_i^T$ and the moments $\boldsymbol{M}_F = [M_x, M_y, M_z]_{ac}^T$ can be deduced thanks to the circulation distributions. The integration of the accelerations $\dot{\boldsymbol{V}}_{K,F} = [\dot{U}_{K,F}, F, \dot{V}_{K,F}, \dot{W}_{K,F}]_i^T$ (in the inertial frame $(ox_iy_iz_i)$) and angular accelerations $\dot{\boldsymbol{\Omega}}_F = [\dot{p}, \dot{q}, \dot{r}]_{ac}^T$ (in the aircraft frame $(ox_{ac}y_{ac}z_{ac})$) allows the integration of the position, attitude and velocity over time:[12]

$$m\dot{\boldsymbol{V}}_{K,F} = \mathbf{F}_F \qquad (10)$$

$$\dot{\boldsymbol{x}}_F = \mathbf{V}_{K,F} \qquad (11)$$

$$\begin{cases} I_x\dot{p} - (I_y - I_z)qr = M_x \\ I_y\dot{q} + (I_x - I_z)pr = M_y \\ I_z\dot{r} - (I_x - I_y)pq = M_z \end{cases} \qquad (12)$$

$$\begin{bmatrix} \dot{\phi} \\ \dot{\theta} \\ \dot{\psi} \end{bmatrix} = \begin{bmatrix} 1 & \sin\phi\tan\theta & \cos\phi\tan\theta \\ 0 & \cos\phi & -\sin\phi \\ 0 & \sin\phi\sec\theta & \cos\phi\sec\theta \end{bmatrix} \begin{bmatrix} p \\ q \\ r \end{bmatrix} \qquad (13)$$

where $[\phi, \theta, \psi]^T$ is the attitude, m is the mass and I_x, I_y, I_z are the products of inertia.

We associate to this complete 6DOF dynamics an autopilot designed to pilot the control commands of the aircraft (i.e. δ_{Ail}, δ_{VT}, δ_{HT} and δ_{Th}). Those control commands modify the aerodynamic loads on the lifting surfaces, which in turn modify the dynamics of the aircraft. The autopilot is designed to make the leader follow a desired target position $\boldsymbol{x}_L^{targ} = [x_L^{targ}, y_L^{targ}, z_L^{targ}]_i^T$ in its environment, and the follower to follow the optimal position in the wake of the leader $\boldsymbol{x}_F^{opt} = [x_F^{opt}, y_F^{opt}, z_F^{opt}]_i^T$; it is much akin to what is done in.[2] For the dynamic part of the model, the variables characterizing the follower's dynamics are therefore

$$\boldsymbol{q}_{dyn} = [U_{K,F}, V_{K,F}, W_{K,F}, x_F, y_F, z_F, p, q, r, \phi, \theta, \psi, \delta_{Ail}, \delta_{VT}, \delta_{HT}, \delta_{Th}] \qquad (14)$$

All those dynamic states are assumed to be measurable by classical onboard equipment of the aircraft, i.e., Inertial Measurement Unit (IMU), Global Navigation Satellite Systems (GNSS), or a good knowledge of the control command dynamics. This makes the estimation strategy completely independent from any additional hardware devices such as pressure or flow sensores used in previous wake tracking strategies.[19,23,28] In addition, measurements of accelerations undergone by the follower as well as aerodynamic angles, i.e., angle of attack α and slip angle β are also deduced from onboard equipments which lead to the true measurement vector

$$\boldsymbol{z} = \left[\dot{U}_{K,F}, \dot{V}_{K,F}, \dot{W}_{K,F}, \dot{p}, \dot{q}, \dot{r}, U_{K,F}, V_{K,F}, W_{K,F}, x_F, y_F, z_F, p, q, r, \phi, \theta, \psi, \delta_{Ail}, \delta_{VT}, \delta_{HT}, \delta_{Th}\right] \qquad (15)$$

that is compared to the predicted measurements vector $\boldsymbol{m}$. The latter gathers the exact same dynamic properties and are computed from the observation operator $\boldsymbol{h}$ from Eq. (1).

3. Wake propagation based on Space Developing and Time Developing simulations

The sensing strategy presented in the previous sections is evaluated in a high-fidelity simulated flight environment that mimic real flight conditions which means, in this work, the nonlinear and unsteady environment produced by the wake of a leader and a follower flying in extended formation. We use a state-of-the-art Vortex-Particle-Mesh (VPM) method[8] to perform LES of the wake flow behind the formation. It combines the advantages of a particle method and of a mesh-based approach which makes it an hybrid approach among the many variants of vortex methods.[29] The method is based on the vorticity-velocity formulation ($\boldsymbol{\omega} - \boldsymbol{u}$) of the Navier-Stokes equations for incompressible flows ($\boldsymbol{\nabla} \cdot \boldsymbol{u}$). It was proven very efficient for the simulation of complex wake flows emanating from wings,[6] wind turbines,[9,10] and rotorcraft[4,5] over long distance.

In this work, we employ a simulation methodology used in[33] and[5] for the study the propagation of aircraft wakes or rotorcraft wakes. We use Space Developing (SD) simulations to accurately reproduce the 3D interactions phenomena occurring during the roll-up of the vortex sheets emanating from the leader and the follower. From these simulations, we generate an initial condition for a Time Developing (TD) simulation, which then allows to study the large scale and long time evolution of the asymmetric wake resulting from the formation. We study a formation flight scenario with two identical aircraft with geometrical properties similar to an A350 or B777 that are reported in Table 1. From those characteristics, we deduce integral properties of the wake of a single aircraft in steady level flight, namely the spacing $b_0 \simeq \frac{\pi b}{4}$ for an elliptic-shaped wing and its intensity Γ_0, i.e.,

$$mg = \rho U_\infty \Gamma_0 b_0 \qquad \rightarrow \qquad \Gamma_0 = \frac{mg}{\rho U_\infty b_0} \qquad (16)$$

Finally, we deduce an estimation of the sinking velocity of the aircraft vortex pair $V_0 = \frac{\Gamma_0}{2\pi b_0}$ and a corresponding time scale $t_0 = \frac{b_0}{V_0}$.

For the SD simulation, the follower is located 15 spans behind a leader in the streamwise direction. This distance ensures the roll-up of the wake without increasing disproportionately the computational domain size, here at $30b \times 4b \times 4b$. Synthetic turbulence, reproducing the spectrum of Homogenous Isotropic Turbulence (HIT), and generated using

DOI: 10.13009/EUCASS2022-6180

	A350		
	Wing	HTP	VTP
Span	$b = 64.5m$	$b_h/b = 0.35.$	$b_v/b = 0.19$
Aspect ratio	$AR = 6.8$	$AR_h = 4$	$AR_v = 4.4$
Shape	Ellipse	Ellipse	Ellipse
Incidence	$\alpha_{0,w} = 4.5°$	$\alpha_{0,h} = 1.3°$	$\alpha_{0,v} = 0°$
Sectional lift slope	$a_0 = 2\pi$	$a_0 = 2\pi$	$a_0 = 2\pi$
Cruise speed		$U_\infty = 250m/s$	
Mass		$m = 300000kg$	
Air density		$\rho = 0.413kg/m^3$	
Zero-lift drag coefficient		$C_{d,0} = 0.01$	

Table 1: Main characteristics of the A350-like aircraft.

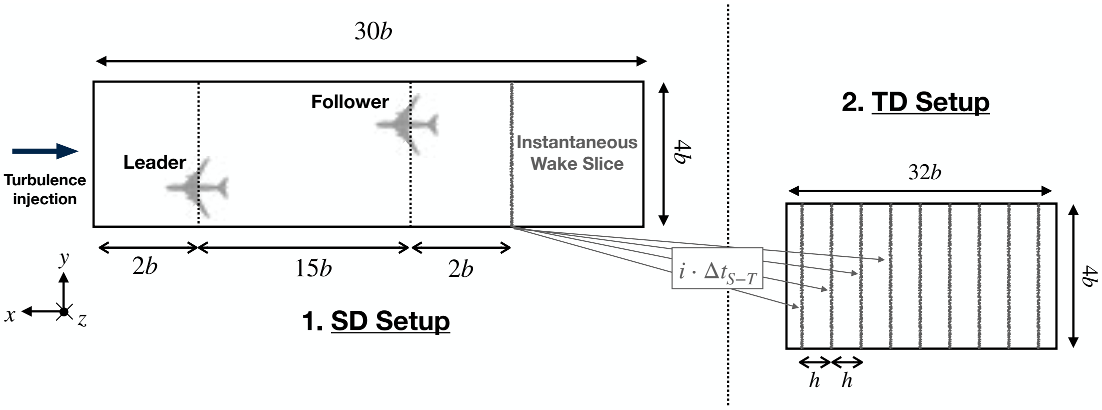

Figure 3: Description of the SD and TD simulation setup.[33]

the Mann algorithm,[27] is injected at the inlet of the computational domain. This affects the wake generation mechanism itself and seeds the flow with perturbations that may trigger instabilities. The turbulence is characterized by an integral length scale $L = 530m$ and a dimensionless Eddy Dissipation Rate (EDR) $\epsilon^* = \frac{\epsilon b_0}{V_0^3} \simeq 2 \cdot 10^{-3}$ corresponding to medium turbulence,[17] which is a reasonable assumption for a formation flight application. In the SD simulation, the leader maintains a fixed target position $\boldsymbol{x}_L^{targ} = [0, -0.5b, 0]$ using the autopilot that controls its control surfaces and thrust, i.e., δ_{Ail}, δ_{VT}, δ_{HT} and δ_{Th}. The follower uses the tracking strategy presented in Section 2 that enables to estimate the position of the leader's wake, i.e., the states $[\hat{y}_{wake}, \hat{z}_{wake}]$. The autopilot of the follower is fed with that estimated position and is instructed to maintain a constant relative position over time, i.e., $[y_F - \hat{y}_{wake}, z_F - \hat{z}_{wake}] = [1.15b, 0]$.

The SD simulation is also used to extract an initial condition for the TD simulation by using the instantaneous vorticity fields observed on a 2D slice normal to the streamwise direction, as described in Fig. 3. We select a 2D slice located 2 spans behind the follower and generate a computational domain of size $L_x \times L_y \times L_z = 32b \times 4b \times 4b$ into which we copy the 2D vorticity filed compute by the SD simulation every step such that $\Delta t_{S-T} = \frac{h}{U_\infty}$ where h is the grid resolution of the mesh used in the simulations. The temporal sampling of the slice observed form the SD simulation associated with the streamwise extent of the TD simulation guarantees to capture the instability modes up to the theoretical fastest-growing Crow mode.[13] To summarize, the SD simulation enables to capture the initial 3D interactions between the leader's wake vortices and the vortex sheet emanating from the trimmed follower, and the TD simulations allows to observe their long-term interactions. The parameters used for both of them are gathered in Table 2.

4. Results

The results section starts with a presentation of the SD simulation of the two-aircraft formation. A 3D visualization of the vorticity is shown in Fig. 4. The vortex sheet emanating of from the leader roll-up into the Leader Outboard Vortex (LOV) and Leader Inboard Vortex (LIV) before reaching the follower. Downstream of the follower, those vortices first interact with the follower's vortex sheet which leads to complex 3D phenomena impacting the roll-up of that same sheet into the Follower Inboard Vortex (FIV) and the Follower Outboard Vortex (FOV).

DOI: 10.13009/EUCASS2022-6180

Space developing	
Domain size ($L_x^{SD} \times L_y^{SD} \times L_z^{SD}$)	$30b \times 4b \times 4b$
Grid resolution	$h/b = 1/64$
Turbulence integral length scale	$L = 530m$
Eddy Dissipation Rate (EDR)	$\epsilon^* = \frac{\epsilon b_0}{V_0^3} \simeq 0.002$
Time developing	
Domain size ($L_x^{TD} \times L_y^{TD} \times L_z^{TD}$)	$32b \times 4b \times 4b$
Grid resolution	$h/b = 1/64$

Table 2: Numerical parameters used in the VPM simulations.

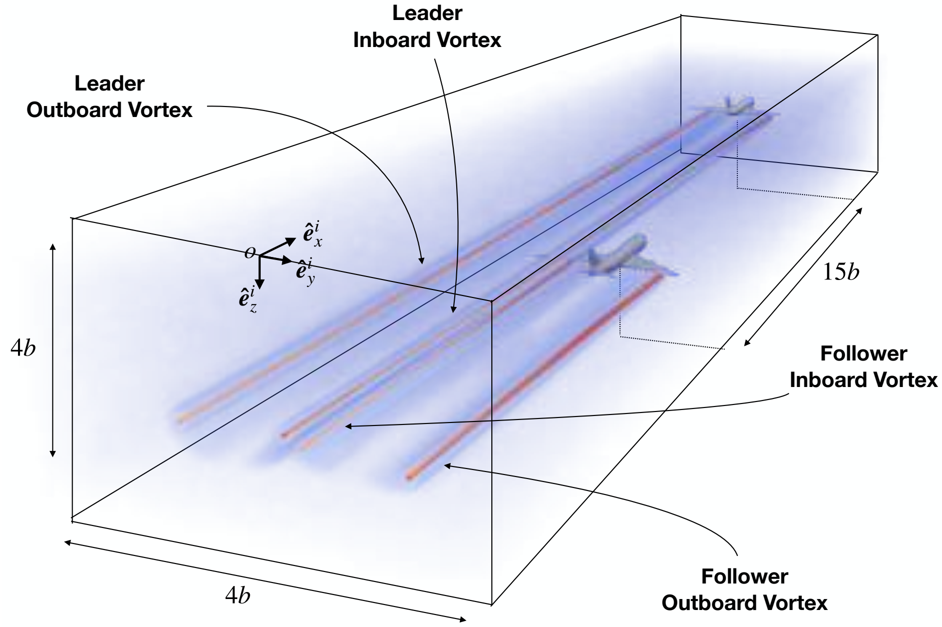

Figure 4: LES numerical setup of the SD simulation: $30b \times 4b \times 4b$ with the leader located $2b$ downstream the inlet, and the follower $15b$ downstream the leader. The mesh is isotropic with size $h/b = 1/64$. Boundary conditions are inflow-outflow in the streamwise direction, i.e., $\hat{\boldsymbol{e}}_x^i$, no-through flow in the two other directions, i.e., $\hat{\boldsymbol{e}}_y^i$ and $\hat{\boldsymbol{e}}_z^i$.

In Section 4.1, we first present results of the estimation strategy performed by the follower in order to track the wake of the leader using the estimator described in Section 2. We then present in Section 4.2 the propagation of the wake that results from the two-aircraft formation, using the simulation methodology described in Section 3.

4.1 Wake tracking

In this section, we observe the performance of the estimator described in Section 2 for the detection of the position of the leader's wake over time. We observe in Fig. 5 the time histories of the estimation of the wake position over time. We use the convective time $t^* = \frac{b}{U_\infty}$ to define a dimensionless time t/t^* in the following graphes.

We observe that the estimator is able to determine the vertical and lateral position of the leader's wake using measurements of its own dynamics. Indeed, except for an initial period during which the estimator converges towards the actual wake position, the estimated position remains within $5 - 10\%$ of the wing span. Also, the confident interval associated to the position and computed as the *a posteriori* variance of the estimate, see Eq. (8) remains within 5%. This accuracy is due to the measurement noise covariance $\boldsymbol{R}$ that is directly related to the accuracy of the onboard measurement. In this work, we assume the estimator deals with accurate measurements which leads to an accurate estimation of the position provided that the surrogate model that is exploited by the estimator accurately models the influence of the leader's wake on the follower's dynamics. We refer to[32] for a more detailed description of the influence of measurement noise on the wake estimation.

In addition to estimating the position of the wake over time, the estimator provides an optimal target position to the autopilot of the follower. Indeed, by maintaining a constant relative position with respect to the estimated leader's

DOI: 10.13009/EUCASS2022-6180

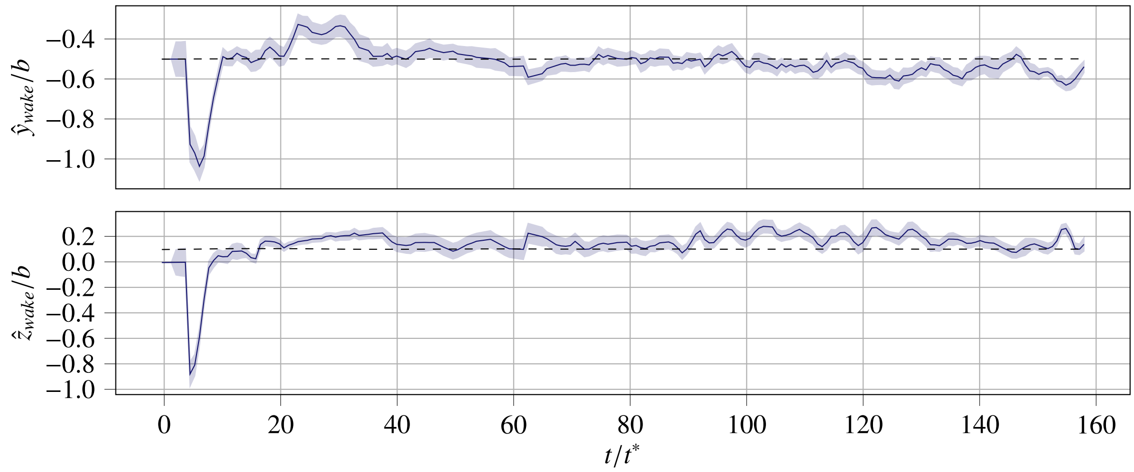

Figure 5: Detection of the wake position. The black dashed line (- -) indicates the actual position of the wake. The blue lines (—) are the estimates with their *a posteriori* confidence interval produced by the EnKF estimator.

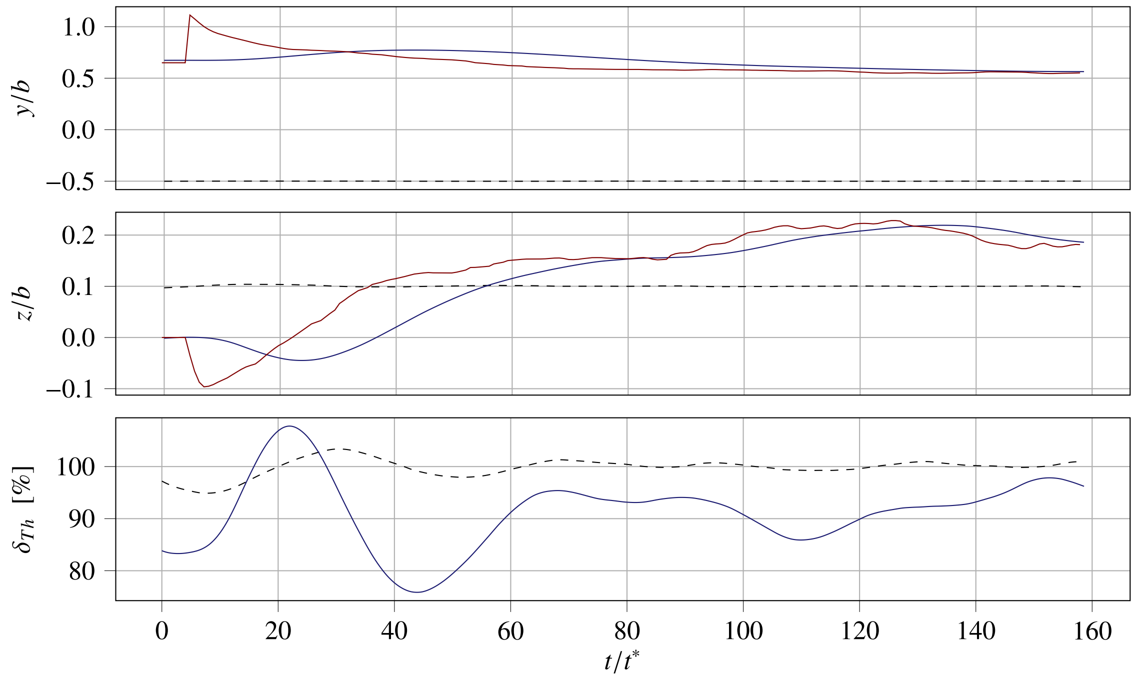

Figure 6: Lateral position (top) and vertical position (middle) of the leader's wake (- -) and of the follower (—). The red lines (—) are the optimal positions computed by the estimator for the follower's autopilot, i.e., $\left[y_F^{opt}, z_F^{opt}\right] = [\hat{y}_{wake} + 1.15b, \hat{z}_{wake} + 0]$. The bottom graphe is the thrust command of the leader (- -) and of the follower (—)

wake position, i.e., $[y_F - \hat{y}_{wake}, z_F - \hat{z}_{wake}] = [1.15b, 0]$, the follower is able to minimize it's energy consumption thanks to the upwash induced by the wake. In Fig. 6, we present time histories of the position of the leader's wake and of the position of the follower. We observe that the follower converges smoothly towards the appropriate lateral position due to the accurate targets that results from the estimation of the lateral position. Because of errors in the estimation of the vertical position, see Fig. 5, the follower does not converges towards the desired position but rather slightly oscillates.

We also present a time history of the thrust commands required by both the leader and the follower in order to maintain the cruise velocity U_∞ along the streamwise direction and the desired positions in the (oy_iz_i) plane, i.e., $\left[y_L^{targ}, z_L^{targ}\right] = [-0.5b, 0]$ for the leader, and $\left[y_F^{opt}, z_F^{opt}\right] = [\hat{y}_{wake} + 1.15b, \hat{z}_{wake} + 0]$ for the follower. We observe that the follower requires about 10% lower thrust compared to the leader which corresponds to values already described in the literature. The thrust required by both aircraft is not constant over time, as the leader needs to compensate the turbulence injected in the domain while the follower tracks the estimated wake position. This makes it moving up or

DOI: 10.13009/EUCASS2022-6180

down which requires different wake intensities.

Fig. 7 present a visual representation of the sensing and tracking methodology. The estimated position converges towards the exact position, then slightly oscillates. The follower moves in order to maintain a constant relative position with respect to that estimated position which leads to an optimized formation flight where the follower tracks the position of the wake without any knowledge of the position of the leader over time.

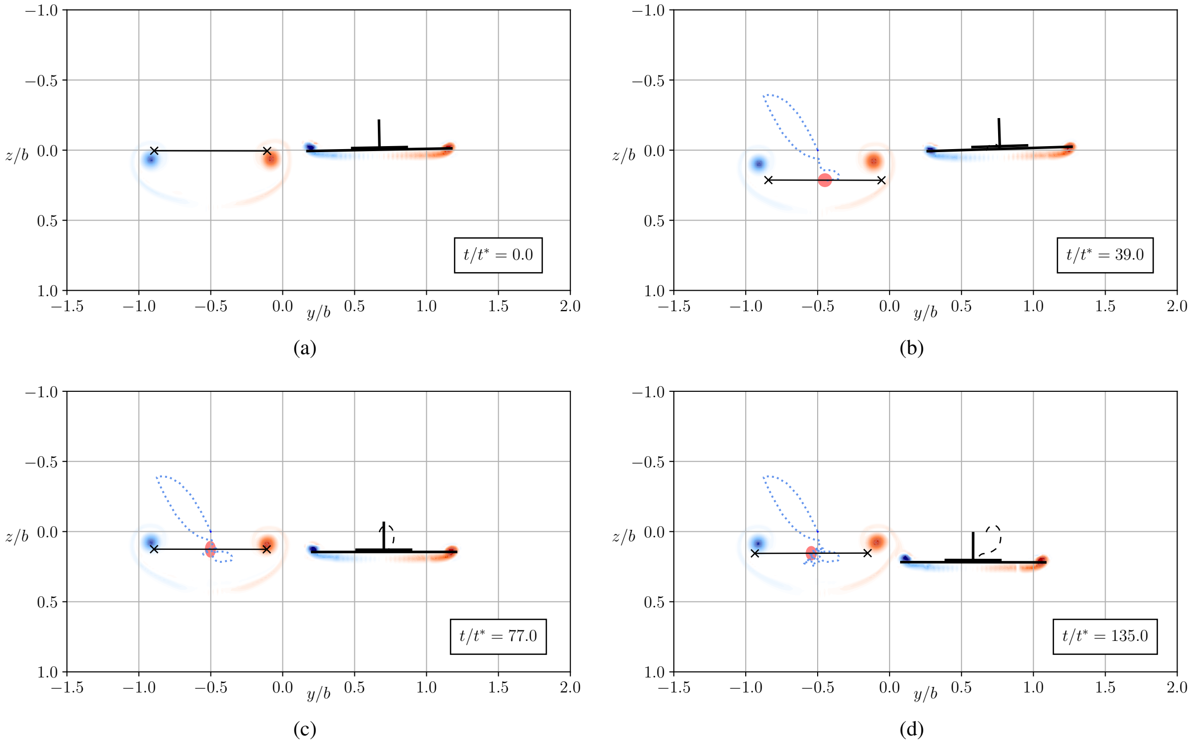

Figure 7: Vortex system estimated over time. The background represents the vorticity behind the follower. The blue dotted line (······) is the history of the estimated position with its confidence interval envelope ( ). The black dashed line (- - -) is the history of the exact position of the follower.

4.2 Wake propagation

In this section, we observe the long-term propagation of the wake emitted by the two-aircraft formation whose follower actively tracks the optimal position in the wake of a leader. Using the methodology described in Section 3 that combines SD and TD simulations, we are able to propagate the wake up to $t = 2 \cdot t_0$, with the reference time $t_0 = \frac{b_0}{V_0}$ that characterizes the sinking convection of the vortex pair of a single aircraft. Fig. 8a is the initial condition that is extracted from a slice located $2b$ behind the follower of the SD simulation presented in Fig. 4 and is propagated over time in order to observe the trajectories and behaviors of the vortices of the system, see Fig. 8.

Initially, the vortices of the formation are mainly straight, with a weak oscillation of the LOV and LIV betraying the impact of the ambient turbulence during the SD simulation. The LIV and LOV are almost totally rolled up and turbulent, unlike the FIV and FOV, between which we still observe a part of the vortex sheet of the follower. The LIV and FIV then move up and towards the right-hand side of the computational domain. This movement is explained by the self-induced velocity of the vortices, by the asymmetry in termes of vortex roll-up and intensity, and by the relative positioning between the aircraft which leads to the rightward displacement. Because of the small distance between the LIV and FIV, a Crow-type oscillating structure rapidly appears. This structure undergo stretching and instabilities of their own, leading to the dissipation of the inboard vortex pair.

The vortices dynamics can be alternatively observed by studying the longitudinally averaged vorticity field $\overline{\omega}_x$ computed using

$$\overline{\omega}_x(y,z,t) = \frac{1}{L_x^{TD}} \int_0^{L_x^{TD}} \omega_x(x_{TD},y,z,t)\,dx_{SD}\ . \ . \tag{17}$$

DOI: 10.13009/EUCASS2022-6180

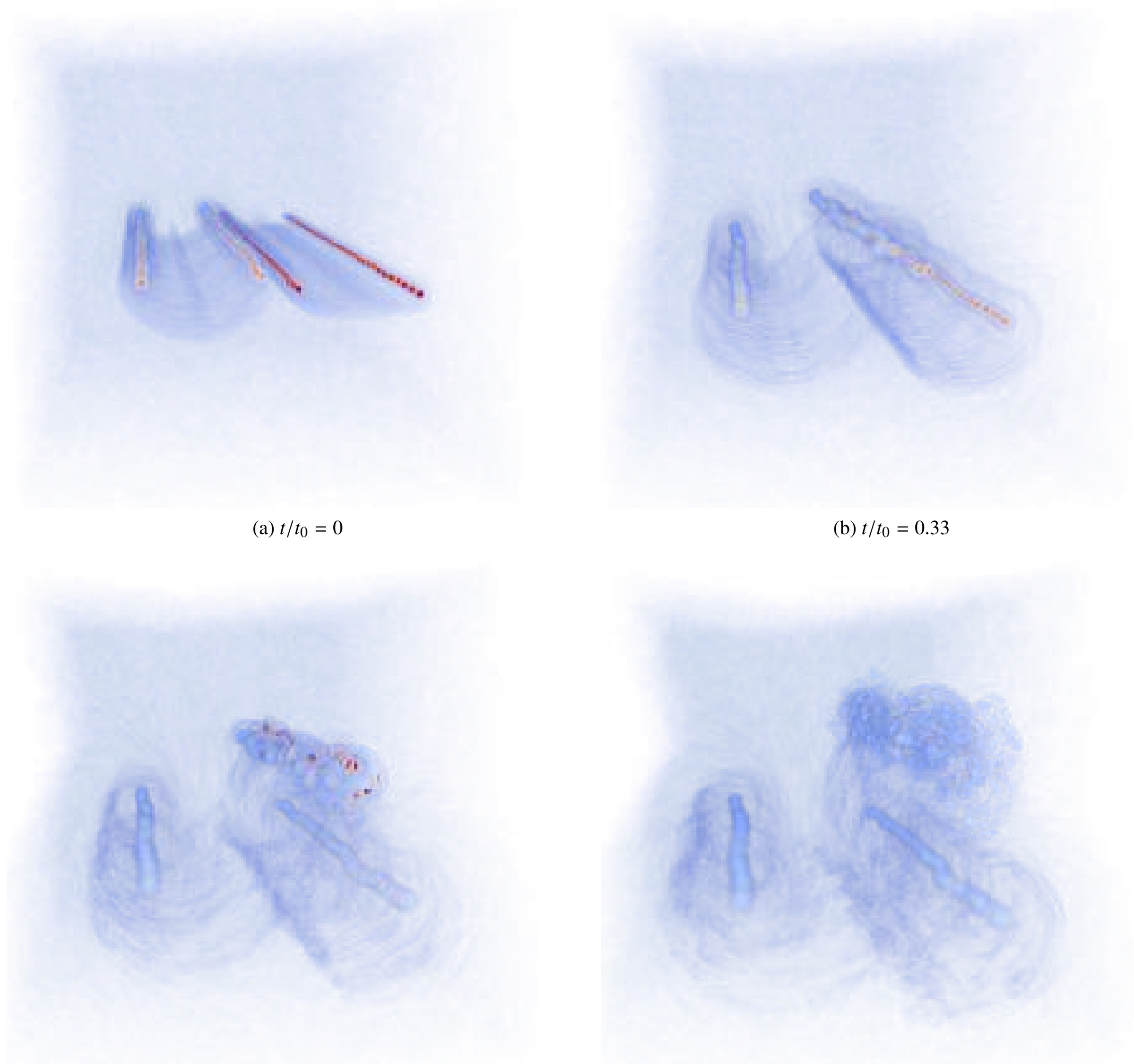

(a) $t/t_0 = 0$ (b) $t/t_0 = 0.33$

(c) $t/t_0 = 0.66$ (d) $t/t_0 = 1.$

Figure 8: Volume rendering of the vorticity at 4 different wakes ages. The initial condition $t/t_0 = 0$ is extracted from a slice located $2b$ behind the follower of the SD simulation presented in Fig. 4.

From the average axial vorticity fields, one might want to compare the trajectories of the wake vortices. In order to measure the mean displacement of the vortices, we compute the position of the vortex centroid using a Gaussian mask, leading to

$$\overline{\omega}_{x,R}(t) = \int_\Omega \frac{1}{\pi R^2} \exp - \frac{\left((y - y_c^a(t))^2 + (z - z_c^a(t))^2\right)}{R^2} \overline{\omega}_x(y,z,t) d\Omega, \tag{18}$$

$$y_c^a(t) = \frac{1}{\overline{\omega}_{x,R}} \int_\Omega \frac{y}{\pi R^2} \exp - \frac{\left((y - y_c^a(t))^2 + (z - z_c^a(t))^2\right)}{R^2} \overline{\omega}_x(y,z,t) d\Omega \tag{19}$$

$$z_c^a(t) = \frac{1}{\overline{\omega}_{x,R}} \int_\Omega \frac{z}{\pi R^2} \exp - \frac{\left((y - y_c^a(t))^2 + (z - z_c^a(t))^2\right)}{R^2} \overline{\omega}_x(y,z,t) d\Omega\ , \tag{20}$$

where Ω is the area covered by the slice (i.e., the $4b$ square), R is a smoothing parameter and $\overline{\omega}_{x,R}$ is the Gaussian-smoothed average vorticity around the vortex centroid in $(y_c^a(\tau), z_c^a(\tau))$. This results in an iterative procedure performed for each one the LOV, LIV, FIV and FOV. The superscript $\cdot^a$ is used to stress that the vortex centroid is obtained relatively to the *average* vorticity field. One observes that this procedure can also be applied to instantaneous vorticity

DOI: 10.13009/EUCASS2022-6180

field $\omega_x^i(y,z,t)$, where i denotes a slice index, rather than average vorticity field $\overline{\omega}_x(y,z,t)$ in order to deduce the position of the instantaneous vortex centroid $\left(y_c^i(t), z_c^i(t)\right)$.

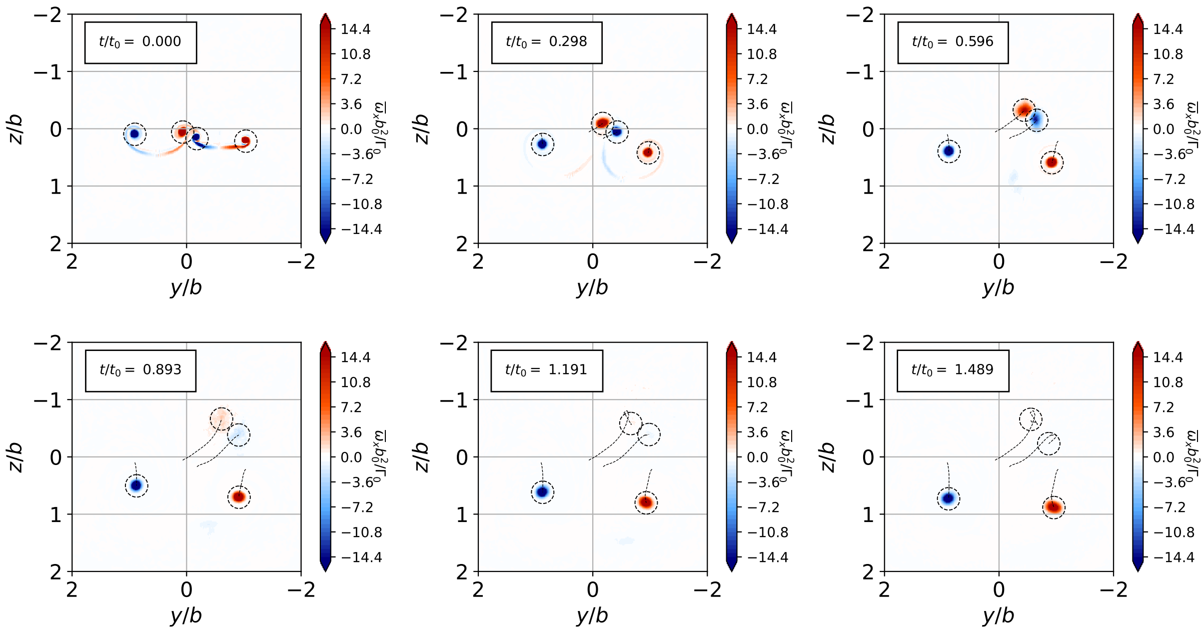

Figure 9: Streamwise average vorticity field $\overline{\omega}_x$ at different age of the wake behind the two-aircraft formation (the follower positions slightly below the leader's wake). The dashed circle indicates the instantaneous position of each vortex while the dashed line is the trajectory.

The averaged axial vorticity fields computed using Eq. (17) is presented in Fig. 9 for several times. We more clearly observe the rightward displacement of the vortex pair made of the LIV and FIV due to their vicinity, their relative initial position and their asymmetry. For $t/t_0 > 0.9$, the mean vortices of the inboard pair seem to have entirely dissipated due to their interaction. On the contrary, the outboard vortices, i.e., LOV and FOV, interact very few and persist in time with a small downward velocity due their self-induced velocity.

As observed in Fig. 8, the dissipation of the inboard vortices is mainly due to the ambiant turbulence that triggers unstable oscillating modes that lead to strong interactions. Therefore, the relative motion of the follower with respect to the wake of the leader induced by the tracking strategy does not seem to be the driving trigger of those oscillations, although it contributes to them. However, the tracking strategy is likely to lead to different relative positions between the follower and the wake of the leader during a formation flight, due to the inherent position uncertainty that the strategy propagates.

In Fig. 10, the evolution of the average vorticity field behind a second two-aircraft formation is presented. In that configuration, the follower positions above the wake of the leader leading to different wake behavior. The vortex pair now move leftwards before dissipating, which shows the strong sensitivity of the wake to the position. During formation flight, both the movement of the leader's wake (,e.g., due to the wind, to the leader's movement, etc) and the movement and the movement of the follower can lead to different relative position that would imply various wake propagation dynamics. This sensitivity to the formation configuration under the uncertainty of a wake tracking strategy opens the way to a more thorough study in terms of impact on the air traffic management.

5. Conclusions

This work presents a simulation strategy that enables to study the impact of a wake tracking strategy on the wake evolution of two aircraft flying in extend formation. This work builds upon[32] and use the estimator designed in that study in order to predict the position of the wake of a leader based on measurements of the dynamics of the follower. This strategy is exploited within a space developing large eddy simulation which enables to capture the roll-up of the vortex sheets originating from the leader and the follower and their mutual interactions. This simulation is combined with a time developing simulation whose initial condition is built from a well-chosen slice in the wake of the two-aircraft formation in order to study the long term evolution of the wake in the turbulent environment.

DOI: 10.13009/EUCASS2022-6180

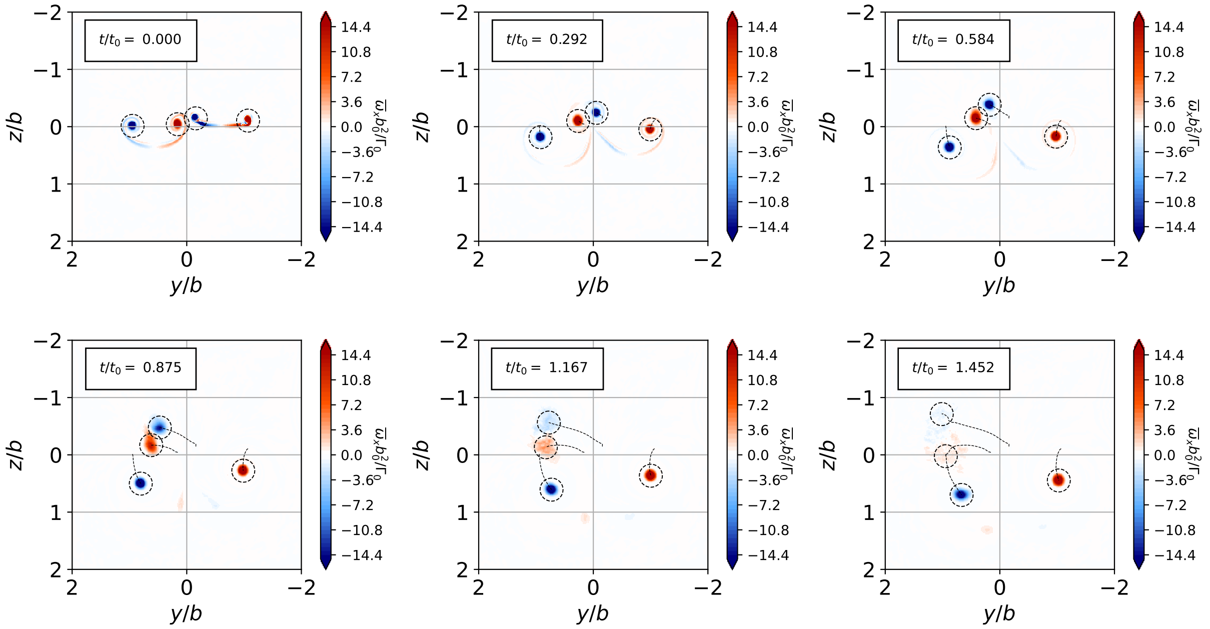

Figure 10: Streamwise average vorticity field $\overline{\omega}_x$ at different age of the wake a second formation flight configuration: the follower positions slightly above the leader's wake. The dashed circle indicates the instantaneous position of each vortex while the dashed line is the trajectory.

The simulations performed highlight the efficiency of the use of dynamic measurements of the follower for the estimation of the position of the leader's wake. The dissipation of the inboard vortices of the resulting formation wake is mostly due to the turbulent environment that triggers instability modes, rather than to the slow relative motion observed between the wake of the leader and the follower. However, the tracking strategy implies different relative positions between the leader's wake and the follower which leads to different wake propagation downstream the formation.

The simulation of more varied formation configurations is considered in futur work in order to quantify in a more global way the impact that formation flight could have. In particular, an appropriate modeling of the uncertainty of the vortex position related to the estimation strategy is envisioned in order to quantify the impact of formation flying on air traffic management through through the design of an operational model of the propagation of aircraft formation wakes.

Acknowledgments

This project has received funding from the European Research Council (ERC) under the European Union's Horizon 2020 research and innovation program (grant agreement no. 725627).

The development work benefited from the computational resources provided by the supercomputing facilities of the UCLouvain (CISM/UCL) and the Consortium des Équipements de Calcul Intensif (CÉCI) en Fédération Wallonie Bruxelles (FWB) funded by the Fond de la Recherche Scientifique de Belgique (F.R.S.-FNRS) under Convention No. 2.5020.11.

References

[1] Airbus. Airbus and its partners demonstrate how sharing the skies can save airlines fuel and reduce co2 emissions, November 2021.

[2] Paolo Binetti, Kartik B. Ariyur, Miroslav Krstic, and Franco Bernelli. Formation Flight Optimization Using Extremum Seeking Feedback. *Journal of Guidance, Control, and Dynamics*, 26(1):132–142, 2015/12/10 2003.

[3] C. Breitsamter. Wake vortex characteristics of transport aircraft. *Progress in Aerospace Sciences*, 47(2):89 – 134, 2011.

DOI: 10.13009/EUCASS2022-6180

[4] Denis-Gabriel Caprace, Philippe Chatelain, and Grégoire Winckelmans. Wakes of rotorcraft in advancing flight: A large eddy simulation study. *Physics of Fluids*, 32(8):087107, 2020.

[5] Denis-Gabriel Caprace and Andrew Ning. Large eddy simulation of the wakes of three urban air mobility vehicles. In *Vertical Flight Society's 78th Annual Forum*, 2022.

[6] Denis-Gabriel Caprace, Grégoire Winckelmans, and Philippe Chatelain. An immersed lifting and dragging line model for the vortex particle-mesh method. *Theoretical and Computational Fluid Dynamics*, 34:21–48, 2020.

[7] Denis-Gabriel Caprace, Gregoire Winckelmans, Philippe Chatelain, and Jeff Eldredge. Wake vortex detection and tracking for aircraft formation flight. In AIAA, editor, *AIAA Aviation 2019 Forum*, June 2019.

[8] Philippe Chatelain, Alessandro Curioni, Michael Bergdorf, Diego Rossinelli, Wanda Andreoni, and Petros Koumoutsakos. Billion vortex particle Direct Numerical Simulations of aircraft wakes. *Computer Methods in Applied Mechanics and Engineering*, 197(13):1296–1304, Feb 2008.

[9] Philippe Chatelain, Matthieu Duponcheel, Denis-Gabriel Caprace, Yves Marichal, and Grégoire Winckelmans. Vortex particle-mesh simulations of vertical axis wind turbine flows: from the airfoil performance to the very far wake. *Wind Energy Science*, 2(1):317, 2017.

[10] Philippe Chatelain, Matthieu Duponcheel, Stephanie Zeoli, Simon Buffin, Denis-Gabriel Caprace, Gregoire Winckelmans, and Laurent Bricteux. Investigation of the effect of inflow turbulence on vertical axis wind turbine wakes. *Journal of Physics: Conference Series*, 854(1):012011, 2017.

[11] David F. Chichka, Jason L. Speyer, Claudio Fanti, and Chan Gook Park. Peak-seeking control for drag reduction in formation flight. *Journal of Guidance, Control, and Dynamics*, 29(5):1221–1230, 2006.

[12] Michael V Cook. *Flight dynamics principles: a linear systems approach to aircraft stability and control*. Butterworth-Heinemann, 2012.

[13] S. C. Crow. Stability theory for a pair of trailing vortices. *AIAA Journal*, 8(12):2172–2179, 1970.

[14] Andre F da Silva and Tim Colonius. A bias-aware enkf estimator for aerodynamic flows. In *2018 Fluid Dynamics Conference*, page 3225, 2018.

[15] Taumi Daniels, William Smith, and Stanislav Kireev. Recent developments on airborne forward looking interferometer for the detection of wake vortices. In *4th AIAA Atmospheric and Space Environments Conference*, page 2791, 2012.

[16] Darwin Darakananda, Jeff Eldredge, Andre da Silva, Tim Colonius, and David R Williams. Enkf-based dynamic estimation of separated flows with a low-order vortex model. In *2018 AIAA Aerospace Sciences Meeting*, page 0811, 2018.

[17] Ivan De Visscher. *Interaction of wake vortices with the atmosphere and the ground : advanced numerical simulation and operational modeling*. PhD thesis, Université catholique de Louvain, 2012.

[18] Ivan De Visscher, Laurent Bricteux, and Grégoire Winckelmans. Aircraft vortices in stably stratified and weakly turbulent atmospheres: simulation and modeling. *AIAA Journal*, 51(3):551–566, 2013.

[19] Levi DeVries and Derek A. Paley. Wake Sensing and Estimation for Control of Autonomous Aircraft in Formation Flight. *Journal of Guidance, Control, and Dynamics*, pages 1–10, 2015/12/09 2015.

[20] Atilla Dogan, Shinya Sato, and William Blake. Flight control and simulation for aerial refueling. In *AIAA guidance, navigation, and control conference and exhibit*, page 6264, 2005.

[21] Geir Evensen. Sequential data assimilation with a nonlinear quasi-geostrophic model using monte carlo methods to forecast error statistics. *Journal of Geophysical Research: Oceans*, 99(C5):10143–10162, 1994.

[22] Tristan C. Flanzer, Stefan R. Bieniawski, and John A. Brown. Advances in cooperative trajectories for commercial applications. In *AIAA Scitech 2020 Forum*, 2020.

[23] Maziar S. Hemati, Jeff D. Eldredge, and Jason L. Speyer. Wake Sensing for Aircraft Formation Flight. *Journal of Guidance, Control, and Dynamics*, 37(2):513–524, 2016/01/25 2014.

DOI: 10.13009/EUCASS2022-6180

[24] Frank Holzäpfel. Probabilistic two-phase wake vortex decay and transport model. *Journal of Aircraft*, 40(2):323–331, 2003.

[25] Mathieu Le Provost and Jeff D Eldredge. Ensemble kalman filter for vortex models of disturbed aerodynamic flows. *Physical Review Fluids*, 6(5):050506, 2021.

[26] P.B.S. Lissaman and Carl A. Shollenberger. Formation flight of birds. *Science*, 168(3934):1003–1005, 1970.

[27] Jakob Mann. Wind field simulation. *Probabilistic Engineering Mechanics*, 13(4):269–282, 10 1998.

[28] D. T. Michel, A. Dolfi-Bouteyre, D. Goular, B. Augère, C. Planchat, D. Fleury, L. Lombard, M. Valla, and C. Besson. Onboard wake vortex localization with a coherent 1.5 μm doppler lidar for aircraft in formation flight configuration. *Optics Express*, 28(10):14374–14385, May 2020.

[29] Chloé Mimeau and Iraj Mortazavi. A review of vortex methods and their applications: From creation to recent advances. *Fluids*, 6(2), 2021.

[30] Andrew Ning, Tristan C Flanzer, and Ilan M Kroo. Aerodynamic performance of extended formation flight. *Journal of Aircraft*, 48(3):855–865, 2011.

[31] Steven J. Portugal, Tatjana Y. Hubel, Johannes Fritz, Stefanie Heese, Daniela Trobe, Bernhard Voelkl, Stephen Hailes, Alan M. Wilson, and James R. Usherwood. Upwash exploitation and downwash avoidance by flap phasing in ibis formation flight. *Nature*, 505(7483):399–402, 01 2014.

[32] Ignace Ransquin, Denis-Gabriel Caprace, Matthieu Duponcheel, and Philippe Chatelain. Wake vortex detection and tracking for aircraft formation flight. *Journal of Guidance, Control, and Dynamics*, 0(0), August 2021.

[33] Ignace Ransquin, Matthieu Duponcheel, and Philippe Chatelain. Dynamics of the wake vortices of a two-aircraft formation, hazard assessment at large distances and sensitivity analysis. In *AIAA SCITECH 2022 Forum*, page 1198, 2022.

[34] S. Unterstrasser and A. Stephan. Far field wake vortex evolution of two aircraft formation flight and implications on young contrails. *The Aeronautical Journal*, 124(1275):667–702, 2020.

[35] Henri Weimerskirch, Julien Martin, Yannick Clerquin, Peggy Alexandre, and Sarka Jiraskova. Energy saving in flight formation. *Nature*, 413(6857):697–698, 2001.